Crystal-Field Effects on the Far-Infrared Cation Vibrations of Transition Metal (2+) Ion Exchanged Faujasite Zeolites

Geoffrey A. Ozin,* Mark D. Baker, John Godber, and Wu Shihua

Contribution from the Lash Miller Chemical Laboratories, University of Toronto, Toronto, Ontario, Canada M5S1A1. *Received June 25, 1984*

Abstract: Fourier-transform far-infrared (FT far-IR) spectra of transition metal ion exchanged faujasite zeolites, $M^{2+}ZY$ (M^{2+} = Ca^{2+}, Mn^{2+}, Fe^{2+}, Co^{2+}, Ni^{2+}, Cu^{2+}, Zn^{2+}; frequency range 350–30 cm^{-1}), are reported for the *first time*. In conjunction with a knowledge of the cation site distribution (X-ray crystallography) and the Brodskii cation vibrational frequency, mass, ionic radius relationship ($\nu_i \propto M_i^{-1/2}R_i^{-3/2}$) it is possible to assign an internally consistent set of far-IR absorptions to cations located in sites I, I′, and III (using standard faujasite notation) of the zeolite lattice. The observed trends in the metal cation vibrational frequencies as a function of the d-orbital occupancy for each site can be adequately rationalized in terms of the effect of d-orbital splitting on the variation of ionic radii with atomic number in a series of high-spin cations of the same charge, residing in the same symmetry environment, taking appropriate account of the influence of the Jahn–Teller effect. On the other hand, low-frequency (300–250 cm^{-1}) cation-sensitive lattice oxygen framework modes are found to exhibit crystal-field effects that are in an "inverse" order to those observed for the corresponding metal cation vibrational modes. The origin of this interesting behavior is also discussed.

Unraveling the electronic and magnetic consequences of d-orbital splitting of transition metal ion exchanged zeolites by optical and electron paramagnetic resonance spectroscopy has generally proven to be a difficult task, mainly because of band overlap complications arising from multiple cation site occupancy.[1] This turns out to be especially obstructive in the case of the broad absorptions that typify the electronic spectroscopy of most transition metal ions.[2a,c] Furthermore, only a few transition metal ions in certain oxidation states and site symmetries have the appropriate electronic ground states to display observable EPR spectra. Of these, spin–orbit coupling, zero-field splitting, and exchange interactions, acting individually or in concert, generally serve to either shift resonances out of the detection range of conventional EPR spectrometers or broaden the resonances to the point that they are either not detectable or convey very little useful information.[2b,c]

In contrast, it is known that the far-IR spectra of alkali and alkaline earth metal ion exchanged zeolites display well-resolved cation vibrational modes (350–30 cm^{-1}) that are characteristic of their site locations in the zeolite framework.[3] Consequently, the far-IR spectra of a series of transition metal cations having the same charge, spin-state (crystal-field), and site symmetry (location) can in principle provide a direct and site-specific probe of the effect of d-orbital splitting on the variation of ionic radii with atomic number when exchanged into a particular zeolite. The approach entails use of the relationship proposed first by Brodskii et al.[3f] between the cation vibrational frequency ν_i for a particular site i and the mass M_i and ionic radius R_i of the cation residing in that site, that is,

$$\nu_i \propto M_i^{-1/2} R_i^{-3/2}$$

This expression derives from the combined use of the diatomic harmonic oscillator approximation for an n-coordinate $M^{q+}O_n$ site, where M^{q+} is assumed to vibrate against an infinite lattice mass, in conjunction with the harmonic M–O bond stretching force constant k, which is related to the M–O bond length through the Badger inverse cube expression.[4] The applicability and usefulness of this simple cation frequency, mass, ionic radius relationship was originally established for alkali and alkaline earth metal ion exchanged faujasites and has more recently found considerable success when applied to the assignment of far-IR cation modes in Ag^+ and Co^{2+} ion exchanged faujasites.[5,6]

In this study we report for the first time the FT far-IR spectra of Ca^{2+}, Mn^{2+}, Fe^{2+}, Co^{2+}, Ni^{2+}, Cu^{2+}, and Zn^{2+} ion exchanged faujasites (Si/Al = 2.50) as well as Co^{2+} faujasites with Si/Al ranging from 1.25 to 20. In most cases X-ray crystallography establishes the cation site distribution and location in the zeolite, and Brodskii's expression greatly assists with the identification of specific cation site vibrational modes. This vibrational information is analyzed in terms of site-specific crystal-field effects as a function of d-orbital occupancy in the above series of divalent metal cations. In a more detailed paper, we will report on the combined use of cation vibrational frequencies and intensities (theory and experiment) for ascertaining metal cation vibrational assignments, site locations, and populations.[7]

Experimental Section

Transition metal ion exchanged zeolites were prepared from sodium zeolite X (Linde 13X; Si/Al = 1.25), sodium Y (Linde LZ-Y52; Si/Al = 2.5), sodium Y(3.8) (Grace, 12489-77 USY; Si/Al = 3.8), and sodium Y(20) (Union Carbide, LZ-20; Si/Al = 20) which had been slurried with 0.1 N NaCl solution to remove sodium defect sites, washed until free of chloride, and calcined in dry oxygen at 500 °C for 16 h. After rehydration, the zeolite was stored over saturated ammonium chloride to maintain a constant humidity. Ion exchange was performed at room temperature with 0.01 N solutions of the chlorides (Mn, Co, Ni, Ca) or nitrates (Cu, Zn) according to standard techniques. In a typical experiment, between 1 and 2 g of the sodium zeolite was weighed out and slurried with 3 L of the corresponding transition metal solution. The pH of the resulting mixture was between 6 and 6.5 and was stirred for 20 h. After filtration the sample was washed until the washings were free of anion (chloride or nitrate) and then dried at 100 °C, lightly ground to a coarse powder, and stored over ammonium chloride. The iron(II) sample was prepared in an analogous fashion from the sulfate; deoxygenated water and low pH (4–5) were used. After exchange the sample was handled under anaerobic conditions.

(1) Mortier, W. J. "Compilation of Extra Framework Sites in Zeolites"; Butterworths: Washington, DC, 1982.

(2) (a) Hoser, H.; Krzysanowski, S.; Trifiro, F. *J. Chem. Soc., Faraday Trans. 1* **1975**, *71*, 665. (b) Heilbron, M. A.; Vickerman, J. C. *J. Catal.* **1974**, *33*, 434. (c) Delgass, W. N.; Haller, G. L.; Kellerman, R.; Lunsford, J. H. "Spectroscopy in Heterogeneous Catalysis"; Academic Press: New York, 1979; and references cited therein.

(3) (a) Butler, W. M.; Angell, C. L.; McAllister, W.; Risen, W. M. *J. Phys. Chem.* **1977**, *81*, 2061. (b) Pilz, W. W.; Peuker, Ch.; Moeller, K.; Kunath, D.; Lohse, U.; Bulau, M.; Samulevic, V. N. *Z. Phys. Chem. (Leipzig)* **1983**, *217*, 264. (c) Peuker, Ch.; Moeller, K.; Kunath, D. *J. Mol. Struct.* **1984**, *114*, 215. (d) Peuker, Ch.; Kunath, D. *J. Chem. Soc., Faraday Trans. 1* **1981**, *77*, 2079. (e) Tabourier, P.; Carru, J. C.; Wacrenier, J. M.; *J. Chem. Soc., Faraday Trans. 1* **1983**, *79*, 779. (f) Brodskii, I. A.; Zhdanov, S. P.; Stanevic, A. E. *Opt. Spectrosc. (Engl. Transl.)* **1971**, *30*, 58.

(4) Badger, R. M. *J. Chem. Phys.* **1934**, *2*, 128; **1935**, *3*, 710.

(5) Ozin, G. A.; Baker, M. D.; Parnis, J. M. *Angew. Chem. Suppl.* **1983**, 1075; Ozin, G. A.; Baker, M. D.; Godber, J. *J. Phys. Chem.* **1984**, *88*, 4902.

(6) Ozin, G. A.; Baker, M. D.; Godber, J. In "Heterogeneous Catalysis"; Shapiro, B., Ed.; Texas A & M University Press: College Station, 1984.

(7) Ozin, G. A.; Baker, M. D.; Godber, J. *J. Am. Chem. Soc.*, in press.

0002-7863/85/1507-1995$01.50/0

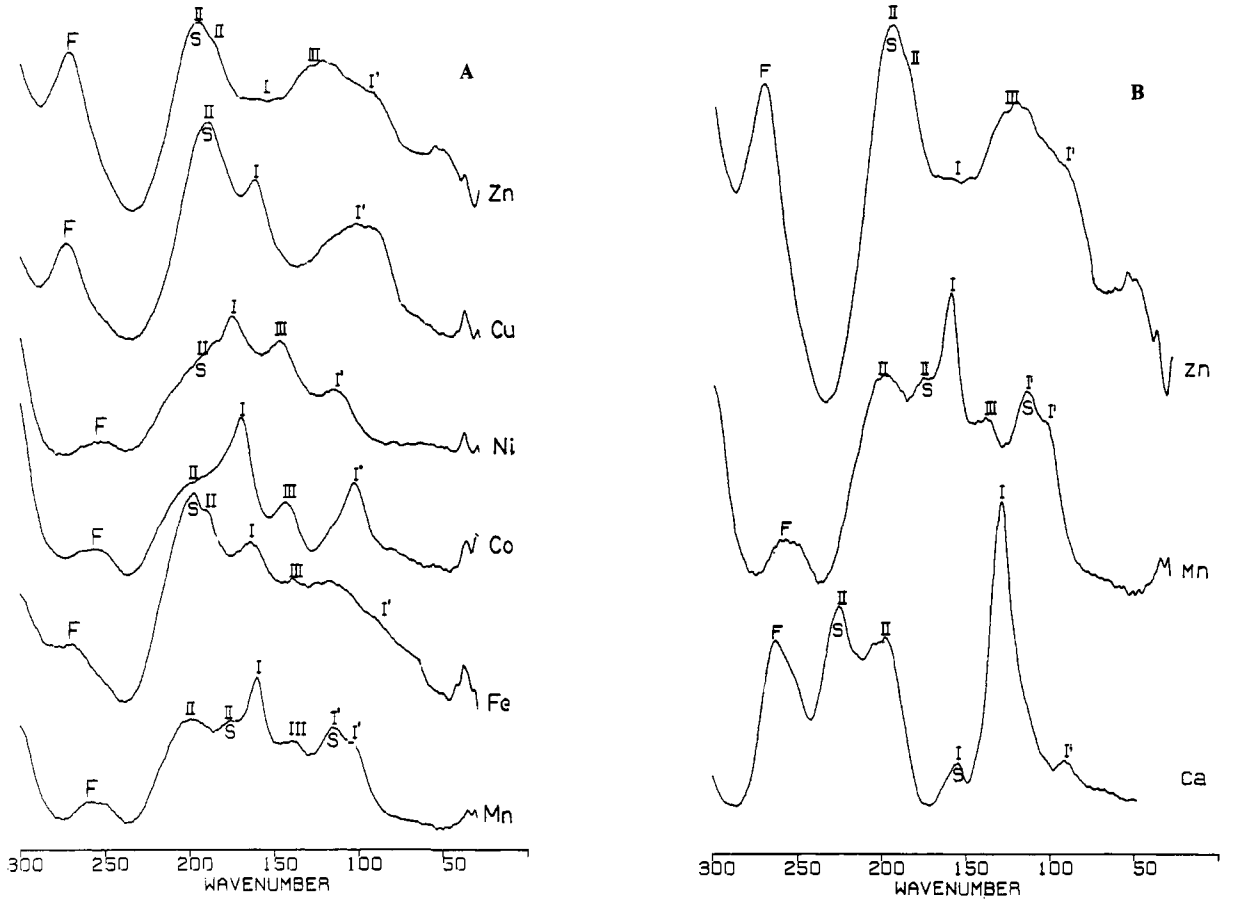

Figure 1. (A) FT far-IR spectra of dehydrated $M^{2+}ZY$ (Si/Al = 2.5) where M^{2+} = Ca^{2+}, Mn^{2+}, Fe^{2+}, Co^{2+}, Ni^{2+}, Cu^{2+}, and Zn^{2+}. The site assignments discussed in the text are shown in standard nomenclature. An S denotes a sodium cation vibration. (B) A more detailed illustration of the d^0, d^5, and d^{10} Ca^{2+}, Mn^{2+}, and Zn^{2+} FT Far-IR data for $M^{2+}ZY$ (Si/Al = 2.5). See ref 7 for greater detail.

The samples were analyzed by inductively coupled plasma emission spectroscopy (ICP) and in some cases by neutron activation at the University of Toronto Slow Poke Reactor Facility. The results of the analyses are as follows (Sample, analytical results): MnY, $Mn_{18.3}Na_{19.4}Y$; ZnY, $Zn_{21.1}Na_{13.8}Y$; NiY, $Ni_{21.2}Na_{13.6}Y$; CaY, $Ca_{21.5}Na_{13}Y$; CuY, $Cu_{13.2}Na_{29.6}Y$; CoX, $Co_{28}Na_{30}X$; CoY, $Co_{17}Na_{22}Y$; CoY(3.8), $Co_{10}Na_{20}Y(3.8)$; CoY(20), $Co_2Na_7Y(20)$; FeY, $Fe_{14.6}Na_{26.8}Y$.

To ensure that the integrity of the zeolite lattice was maintained after exchange, the samples have been studied by powder X-ray diffraction and compared to the starting material. No evidence has been found for any alterations of the zeolite lattice.

The zeolite samples were pressed into self-supporting wafers by using between 5 and 8 tons $in.^2$. The wafers were clamped into the sample holder of an in situ vacuum cell that was mounted in the vacuum chamber of a Nicolet 200SXV FT far-IR spectrometer. The sample wafers could be moved within their own vacuum system to intersect the IR beam or to a furnace area where dehydration or reaction chemistry could be performed over the range of 10 to ca. 600 °C. Spectra were recorded with a 6.25-μm Mylar beam splitter and TGS detector. The spectra reported are the result of the coaddition of 500 interferograms resulting from a 30-min collection time. Survey spectra of useable quality could be obtained in less than a minute. The spectral resolution is 4 cm^{-1} and the spectra have not been smoothed in any way; however, they have been base line corrected. After thermal or chemical treatment the samples were cooled to room temperature or below before recording the spectra.

Results and Discussion

In this paper we will be concerned only with the far-IR spectra of the 400–500 °C dehydrated $M^{2+}ZY$ samples for Ca^{2+}, Mn^{2+}, Fe^{2+}, Co^{2+}, Ni^{2+}, Cu^{2+}, and Zn^{2+}. The completely hydrated $M^{2+}ZY$ samples represent a distinct problem that will form the subject of another study. Typical traces of the dehydrated samples are shown in Figure 1. By examination of the compilations of Mortier,[1] one can determine that at the transition metal ion exchange level used for these recordings, except for Mn^{2+}, the residual Na^+ cations reside exclusively in site II located in front of a six-ring in the α-cage (Figure 2). These have been previously established to absorb in the far-IR within the characteristic frequency range 200–190 cm^{-1} and are easily assigned as indicated by Na^+, S(II) in Figure 1. The spectra of unexchanged Na^+ZY have been assigned quite satisfactorily for sites I, I′, II, and III.[3] By use of these Na^+ cation frequencies and Brodskii's expression, it has proven possible to satisfactorily identify cation site modes

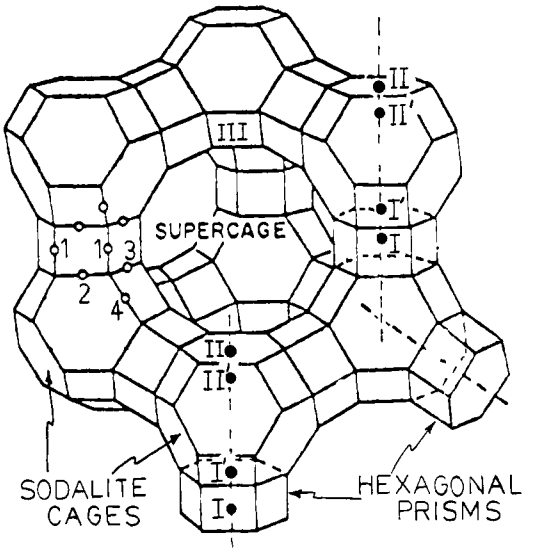

FAUJASITE

Figure 2. Perspective view of faujasite zeolite Y. The four crystallographically distinct framework oxygens are indicated on the figure along with specific cation sites as discussed in the text.

Table I. Observed and Calculated M^{2+} Cation Frequencies for $M^{2+}ZY$[a]

	Ca^{2+}	Mn^{2+}	Fe^{2+}	Co^{2+}	Ni^{2+}	Cu^{2+}	Zn^{2+}
site I							
obsd	130.6	160.7	165	170	176.5[b]	163	162
calcd	135.0	149.2	160.4	165.5	176.5[b]	160.9	154.4
site I′							
obsd	91.2	115.9	100	104	116.3[b]	103	100
calcd	88.9	98.2	105.7	109.0	116.3[b]	106.0	101.8
site III							
obsd		140.2	139.5	142	148.1[b]	~137	126
calcd	113.3	125.2	134.6	138.9	148.1[b]	135	129.6
"lattice oxygen framework" mode	262.7	257	269	258	252	273	271

[a] High-spin metal cation sites. [b] Reference cation frequency.

Table II. Ionic Radii and Atomic Masses of High-Spin, Octahedral, Divalent Transition Meal Cations

	Ca^{2+}	Mn^{2+}	Fe^{2+}	Co^{2+}	Ni^{2+}	Cu^{2+}	Zn^{2+}
$r_{M^{2+}}$[a], Å	1.14	0.96	0.91	0.875	0.84	0.87	0.885
M	40.08	54.938	55.847	58.9332	58.71	63.546	65.38

[a] Reference: Adams, D. M. "Inorganic Solids"; Wiley: New York, 1974.

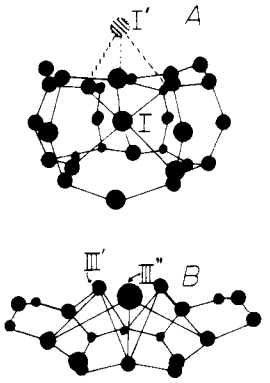

Figure 3. (A) Perspective representation of the coordination of the site I and I′ M^{2+} cations in dehydrated $M^{2+}ZY$. (NB sites I and I′ are never simultaneously occupied.) (B) Perspective drawing of the site III′ and III″ M^{2+} cations at the sequence of four rings in dehydrated $M^{2+}ZY$. (NB sites III′ and III″ are never simultaneously occupied.)

in Ag^+ and Co^{2+} ion exchanged faujasites.[5,6] In particular, for $Co^{2+}ZY$, site I, III, and I′ cation vibrations were assigned to well-resolved far-IR absorptions at 170, 142, and 104 cm^{-1}, respectively. These are indicated in Figure 1 with the respective Roman numerals. Illustrations of the detailed structure for sites I, III, and I′ are shown in Figure 3 and will be discussed later in reference to the d-orbital splitting patterns for the different cation site symmetries. Surveyance of the observed cation modes of the Ca^{2+}, Mn^{2+}, Fe^{2+}, Co^{2+}, Ni^{2+}, Cu^{2+}, and Zn^{2+} exchanged zeolites below the Na^+ (II) absorption (200–190 cm^{-1}) reveals three major absorptions (with some additional superimposed smaller band splittings) in all cases except for $Cu^{2+}ZY$ where the middle band of the major triplet absorption is not as well resolved. Qualitatively, these three bands in order of decreasing frequency would appear to be associated with the cation vibrational modes of sites I, III, and I′, respectively, as listed in Table I.[7]

At this stage the Brodskii expression becomes particularly helpful in conjunction with the crystallographically established cation site distributions listed in ref 1. In Figure 4A and Table

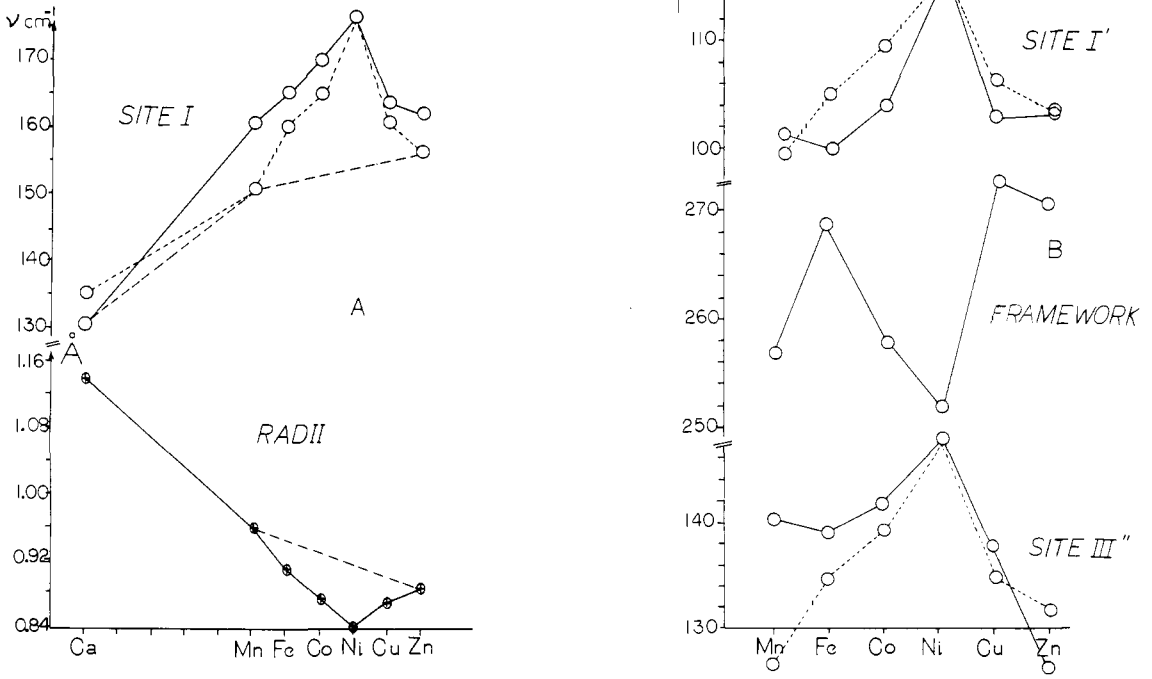

Figure 4. (A) Graphical representation of the observed (—) and calculated (- - -) cation vibrational frequencies for cations in site I as a function of atomic number along with the variation in ionic radii (see Table II) for high-spin octahedral divalent transition metal cations. (B) Graphical representation of the observed (—) and calculated (- - -) vibrational frequencies for sites I′ and III cations and the cation-sensitive framework mode (300–250 cm^{-1}) discussed in the text. The so-called "inverse crystal-field effect" can be clearly seen for the framework mode.

II the variation in cationic radii for M^{2+} transition metal ions with atomic number in the series Ca^{2+}, Mn^{2+}, Fe^{2+}, Co^{2+}, Ni^{2+}, Cu^{2+}, and Zn^{2+} are plotted and listed respectively. These ionic radii refer to high-spin state, divalent cations in octahedral environments (noting that it is impossible to obtain the Jahn–Teller unstable Cu^{2+} in a truely octahedral site, thus rendering the assessment of their "octahedral" radii somewhat uncertain). By fixing the three observed cation vibrational modes of e.g., $Ni^{2+}ZY$, as being characteristic of Ni^{2+} in sites I, III, and I′, respectively,[7] and by employing the Brodski expression, one can estimate the corresponding cation frequencies for Ca^{2+}, Mn^{2+},Fe^{2+},Co^{2+},Cu^{2+}, and Zn^{2+} in sites I, III, and I′. These calculated frequencies together with the respective observed values are represented graphically in Figure 4A,B.

In the case of site I M^{2+} cations, although the agreement between the observed and calculated cation frequencies is not exact, the trend in the values with atomic number is clearly reproduced, that is, a monotonically increasing function from Mn^{2+} to Fe^{2+} to Co^{2+} to Ni^{2+} with a dramatic dropoff at Cu^{2+} and a further small decrease at Zn^{2+}. The fact that this frequency–atomic number correlation actually exists and parallels in an *inverse* manner the trend in the respective ionic radii (Figure 4A) provides extremely compelling evidence for invoking crystal-field contributions to the far-IR cation vibrations of transition metal $M^{2+}ZY$ systems.

At this point, some of the details concerning the cation sites of lower symmetries deserve discussion in terms of their anticipated and observed frequency–atomic number behavior, band splittings, and possible Jahn–Teller effects.

Examination of Figure 3 shows that the local site symmetry of cations in site I′ (residing over three O(3) oxygen atoms of a hexagonal six-ring in the β-cage) is C_{3v}, neglecting the effect of the Si/Al distribution in the zeolite lattice[8] (next-nearest-neighbor Si/Al perturbation effects of this kind are expected to be small). For this site, two $\nu(MO_3)$ cation vibrations are IR active (A_1 + E), of which the degenerate E mode is expected to be the most intense. It is the presence of the weaker symmetric A_1, $\nu(MO_3)$ cation mode (together with a possible smaller Si/Al perturbation splitting) that is thought to be responsible for the broad, asymmetric (sometimes split) appearance of the site I′ cation band in the region 100–116 cm^{-1} (Figure 1). It is the average value of these split site I′ bands that is plotted in Figure 4B.[7]

For low-symmetry sites, such as those formed on the surface of catalysts and in zeolites, the d-orbital energy levels have been calculated and fitted to experimental optical spectra. In particular, Klier and co-workers[13] have performed such calculations for d^1–d^9 metal cations in a C_{3v} ligand field made up of three lattice oxygens as found in site I′ of crystalline zeolites. This site together with the corresponding d-orbital splitting diagram is shown below; the symmetry types of the various levels are indicated:

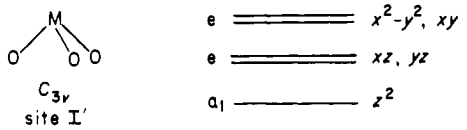

From the calculated and observed electronic spectra of transition-metal cations in site I′, it has been deduced that the oxygens of the zeolite lattice are "weak" ligands and all the metal cations are in their high-spin state.[13] Thus for a Mn^{2+} high-spin C_{3v} MO_3 site I′ species, the d-orbital manifold is half-occupied (spherical). The next three electrons can be seen to occupy $a_1(z^2)$ and $e(xz, yz)$ d orbitals whose spatial extent is such that they tend either to lie away from or reside between the M–O bonds. Because the shielding of one d electron by another from the nuclear charge is imperfect, a steady contraction in the ionic radii on passing from site I′ Mn^{2+} to Fe^{2+} to Co^{2+} to Ni^{2+} is expected as found for site I cations. The d electrons in Fe^{2+}, Co^{2+}, and Ni^{2+} are thus not spherically distributed about the nuclei, and therefore their ionic radii are expected to all lie below a reference curve passing through those of the spherical cations Ca^{2+}, Mn^{2+}, and Zn^{2+} (Figure 4A) in an analogous manner to that found for octahedral site I M^{2+} cations.[9] However, when the next electron at Cu^{2+} is added, it enters the $e(x^2-y^2,xy)$ d-orbital set which is concentrated in those regions of space closer to the M–O bonds. Thus compared to the effect of the $a_1(z^2)$ and $e(xz, yz)$ electrons (which provide little shielding between the positive metal ion and the negative oxygen ligands causing a larger contraction of the M–O bonds than would have occurred had the d electrons been spherically distributed) the $e(x^2-y^2, xy)$ electron in Cu^{2+} provides a great deal more screening than would be provided by spherically distributed electrons and causes the radius to actually increase relative to Ni^{2+}. In brief, the effect of d-orbital splitting on the variation of ionic radii with atomic number is expected to be essentially the same for an O_h site I and C_{3v} site I′ high-spin metal cation. Thus it is not surprising that the overall cation vibrational frequency–atomic number correlation observed for site I′ cations shows a marked resemblance to that found for site I cations (Figure 4). Credence for the existence of a Jahn–Teller effect on site I′ Cu^{2+} stems from the broad structured appearance of the site I′ Cu^{2+} band (Figure 1); it is here that Cu^{2+} in the C_{3v} MO_3 site is expected to be subject to a Jahn–Teller distortion (occupancy of the degenerate $e(x^2-y^2, xy)$ d orbitals) toward a C_s symmetry MO_3 site (e-type vibrational distortion mode).

It remains to discuss the observed frequency–atomic number trend for the site III cations shown in Figure 4. These cations reside over the four-rings of the large cavity (sites III′ and III″ shown in Figure 3). No simultaneous occupancy of two adjacent sites III′ or III″ is expected. The local symmetry of these sites is C_s, although for vibrational purposes site III′ can be considered to have pseudo-C_{4v} symmetry. From a vibrational point of view, site III′ in C_{4v} symmetry has A_1 + B_1 + E $\nu(MO_4)$ cation modes, of which the A_1 + E are IR active, with the asymmetric E mode expected to have the greater IR intensity. Site III″ cations in C_s symmetry have 2A′ + A″ $\nu(MO_3)$ cation modes, of which the asymmetric A″ is likely to be the most intense, with some slight IR activity from at least one of the A′ modes. Thus the site III cation modes (neglecting any next-nearest-neighbor effects from the Si/Al distribution around site III) are expeted to appear as single bands (E or A″) with some possible broadening or splitting contributions from the respective symmetric cation modes (A_1 or A′). Experimentally one can conclude that if the aforementioned symmetric $\nu(MO_n)$ cation modes contribute to site III, the effect is weak, as the site III cation absorption (139–148 cm^{-1}) appears as a single band (Figure 1). It is also noteworthy that the site III cation band is either absent or not well resolved in $Cu^{2+}ZY$ (Figure 1); only the former would be consistent with crystallographic studies for samples similar to those used in this study.[11] Similar arguments to those expounded for site I and I′ regarding the effect of d-orbital splittings on the variation of ionic radii with atomic number are expected to also hold true for high-spin, site III cations. This appears to be borne out in practice as seen from the overall resemblance of the cation vibrational frequency–atomic number trends for all three metal cation sites, I, I′, and III (Figure 4).

Collecting together these ideas, we can conclude that although some slight irregularities exist for the metal cation vibrational modes corresponding to the lower symmetry lattice sites I′ and III (Figure 4B), probably originating from, for example, small O–M–O angular variations and Jahn–Teller distortions, similar kinds of crystal-field effects nevertheless appear to be operative for these sites as observed for site I cations (Figure 4A). This can be judged from the overall similarity of the trends in the cation

(8) Engelhardt, G.; Lippmaa, E.; Mägi, M. *J. Chem. Soc., Chem. Commun.* **1981**, 712 and references cited therein.
(9) Cotton, F. A.; Wilkinson, G. In "Advanced Inorganic Chemistry"; Interscience: New York, 1972.
(10) Gellens, L. R.; Mortier, W. J.; Uytterhoeven, J. B. *Zeolites* **1981**, *1*, 11 and references cited therein.
(11) Gallezot, P.; Taarit, Y. B.; Imelik, B. *C. R. Hebd. Seances Acad. Sci., Ser. C* **1971**, *272*, 261.
(12) Moran, D. R. *Phys. Rev.* **1969**, *179*, 846. Sturge, M. D. *Solid State Phys.* **1967**, *20*, 91. Engleman, R. "The Jahn–Teller Effect in Molecules and Crystals"; Wiley: New York, 1972; and references cited therein.
(13) Klier, K.; Hutta, P. J.; Kellerman, R. *ACS Symp. Ser.* **1977**, *No. 40*, 108.

Table III. Observed Cation Vibrational Frequency Dependence for Site I Co^{2+} Ion Exchanged Faujasite Zeolites on the Si/Al Ratio

Si/Al	frequency, cm^{-1}
1.25	175.5
2.5	170
3.8	168
20.0	164

vibrational frequencies for Ca^{2+}, Mn^{2+}, Fe^{2+}, Co^{2+}, Ni^{2+}, Cu^{2+}, and Zn^{2+} cations residing in sites I, I′, and III as well as the reasonable agreement between their observed and calculated values (Figure 4A,B; see ref 7 for further details).

We wish to point out that cation-sensitive absorption bands for alkali ion exchanged faujasites have been previously observed in the range 300–250 cm^{-1} and have been variously ascribed to pore opening motions of the zeolite lattice, framework oxygen modes or have remained unassigned.[3] In the present study of $M^{2+}ZY$, where M^{2+} = Ca^{2+}, Mn^{2+}, Fe^{2+}, Co^{2+}, Ni^{2+}, Cu^{2+}, or Zn^{2+}, we have also observed for each sample a single absorption in this region whose frequency is not only cation sensitive but also displays a trend with atomic number (Figure 4) that is just the "inverse" of that shown by the cation site I′ vibration observed between 100 and 120 cm^{-1} (Figure 4). This observation carries pivotal clues as to the exact nature of the cation-sensitive modes in the 300–250-cm^{-1} range. If one considers the model of a M^{2+} cation residing in site I′ interacting with three oxygen atoms of a hexagonal six-ring,

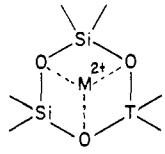

T = Si or Al

then from a crystal-field point of view one can envisage that a Coulombic interaction between the M^{2+} and the oxygens should result in a concomitant reduction in the Si–O and/or Al–O bond strengths of the adjacent six-ring; that is, greater charge transfer from oxygen to M^{2+} drains electronic charge density from the six-ring thereby weakening the framework bonds. When this concept is coupled with the variation in cation ionic radius with atomic number (Table II), one can begin to understand the origin of the inverse frequency–atomic number relationship observed for the bands in the 300–250-cm^{-1} region and the site I′ cation modes. On these grounds we favor the assignment of cation-sensitive bands in the 300–250-cm^{-1} range in terms of six-ring framework vibrations interacting with a cation, rather than pore-opening modes.

On a final note, it is interesting to extend the concepts outlined above to the question of the cation vibrational dependence on the Si/Al ratio for a series of faujasites. In order to investigate these effects we have prepared a series of Co^{2+} faujasites having Si/Al ratios of 1.25, 2.5, 3.8, and 20. In Figure 5A,B the far-IR spectra of the sodium and the Co^{2+} ion exchanged forms of these zeolites are presented. It is a straightforward matter to identify the residual sodium cation modes (even at Si/Al = 20:1), and by logical deduction the respective Co^{2+} cation modes are indicated with the usual nomenclature in Figure 5B.

By examination of trends in the corresponding cation frequencies, it is immediately apparent that each cation site vibration tends to red shift with increasing Si/Al ratio, which is synonomous with decreasing charge density (basicity) on the framework oxygens (an interesting new way of directly probing metal-support effects). In essence one is observing the effect of a diminishing framework crystal field on the individual cations. This is shown for site I Co^{2+} in Table III, from which a relationship between cation frequency and Si/Al ratio clearly exists. It is particularly noteworthy that site I Co^{2+}, as expected, is the majority site as judged by its absorbance and is in fact the only detectable site in the high silica faujasite, Si/Al = 20:1 (Figure 5B). These observations can be considered to provide additional support for the crystal-field model for M^{2+} zeolites.

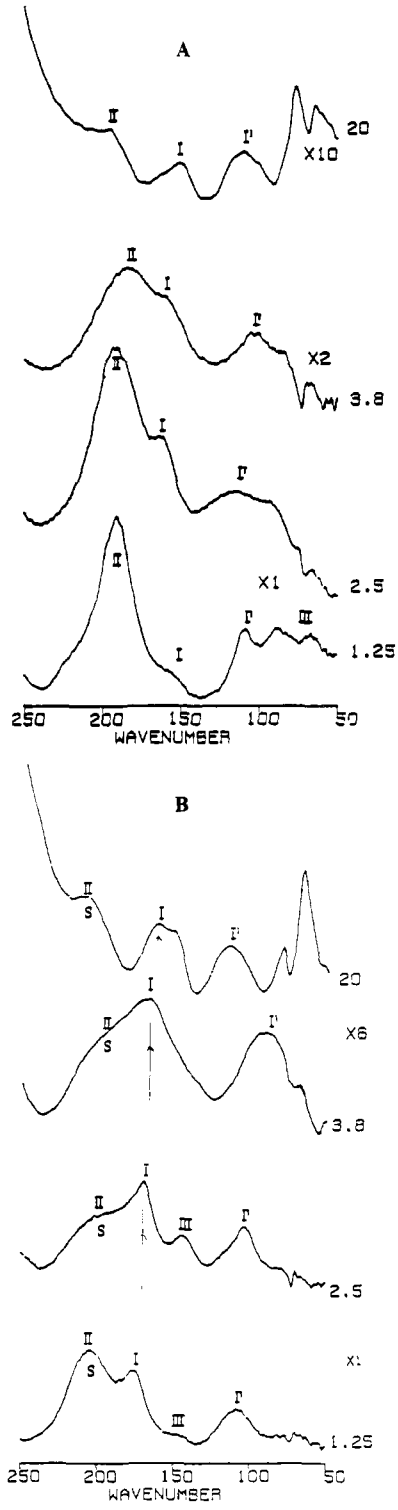

Figure 5. (A) Far-infrared absorbance spectra of dehydrated sodium faujasite zeolites with the Si/Al ratio indicated. The top two spectra are on a ×10 and ×2 expansion. (B) Far-infrared absorbance spectra of dehydrated Co^{2+} ion exchanged faujasite zeolites with different Si/Al ratios. Note that the top two traces are on ×6 expansion. The numbers beside the figures refer to the Si/Al ratio of the zeolite. The formulas of the samples are as follows: Si/Al (1.25), $Co_{28}Na_{30}ZX$; Si/Al (2.5), $Co_{17}Na_{22}ZY$; Si/Al (3.8), $Co_{10}Na_{20}ZY$; Si/Al(20.0), Co_2Na_7ZY.

Conclusion

Far-IR spectroscopy provides a highly sensitive, direct, and site-specific probe of crystal-field effects in transition metal ion exchanged faujasite zeolites. With the ability to easily assign the vibrational frequencies associated with specific cation sites (essentially a group frequency approach), it now becomes feasible to monitor the effects of, for example, alterations in the Si/Al

ratio and number and type of residual alkali cations on the charge density residing on the oxygen atoms in the zeolite framework, all of which contribute to the crystal field sensed by, and the electron density located on, the transition metal cation. Ultimately this knowledge could assist with the understanding of metal-support effects and in the fine tuning of the electronic, magnetic, chemical and catalytic properties of transition metal loaded zeolites.

Acknowledgment. The financial assistance of the Natural Sciences and Engineering Council of Canada's Strategic Grants Programme and the Connaught Foundation of the University of Toronto is gratefully appreciated. The granting of a 3M Corp. scholarship and a Union Carbide Innovation Recognition Award to G.A.O proved to be invaluable. In addition, the donation of zeolite samples from, and helpful technical discussions with, Dr. Edith Flanigen (Union Carbide), Dr. Nicolas Spencer (W. R. Grace Co.) and Dr. Paul Kasai (IBM) is sincerely appreciated. W.S. is also indebted to Nankai University and the Government of the Peoples Republic of China for a 2-year leave of absence at the University of Toronto and financial assistance. We are indebted to Kate Helwig for preparation of the calcium sample.

Registry No. Ca^{2+}, 14127-61-8; Mn^{2+}, 16397-91-4; Fe^{2+}, 15438-31-0; Co^{2+}, 22541-53-3; Ni^{2+}, 14701-22-5; Cu^{2+}, 15158-11-9; Zn^{2+}, 23713-49-7.

Epoxidation of Olefins by Cytochrome P-450 Model Compounds: Kinetics and Stereochemistry of Oxygen Atom Transfer and Origin of Shape Selectivity

James P. Collman,*[1a] John I. Brauman,*[1a] Bernard Meunier,[1b] Teruyuki Hayashi,[1a] Thomas Kodadek,[1a] and Scott A. Raybuck[1a]

Contribution from the Department of Chemistry, Stanford University, Stanford, California 94305, and the Laboratoire de Chimie de Coordination du Centre National de la Recherche Scientifique, 31400 Toulouse, France. *Received August 10, 1984*

Abstract: An analysis of the mechanism of the lithium hypochlorite epoxidation of olefins catalyzed by Mn(TPP)Cl is presented. We have previously reported that the oxygen atom transfer from manganese porphyrin to olefin occurs via an oxo-olefin intermediate whose breakdown is the rate-determining step of the catalytic cycle. Stereochemical and kinetic evidence presented here indicate that both formation of this intermediate and its subsequent breakdown to form epoxide are, in general, concerted processes. The rarely observed loss of stereoselectivity represents the presence of a minor leakage pathway in the breakdown of the oxo-olefin complex to form epoxide. Shape selective olefin epoxidation is achieved when the sterically hindered porphyrin, Mn(TMP)Cl, is used as a catalyst in the hypochlorite system. The observed shape selectivity parallels the large differences in binding energies for formation of the oxo-olefin complex.

Introduction and Background

The cytochrome P-450 enzyme family catalyzes the reaction of hydrocarbons with molecular oxygen, incorporating one oxygen atom into the substrate, the other being reduced to water[2] (eq 1).

$$RH + O_2 + NADPH + H^+ \rightarrow ROH + H_2O + NADP^+ \quad (1)$$

The active site contains an iron(III) protoporphyrin IX moiety with a cysteine thiolate as one axial ligand. Evidence to date indicates that the active species is an iron oxo complex in which the iron porphyrin system is two oxidation levels above the ferric state. The reactivity of this high-valent species is remarkable, P-450 being the only known hemoprotein capable of hydroxylating unactivated carbon–hydrogen bonds. The majority of steps in the catalytic cycle of the enzyme are reasonably well understood. However, the mechanism of the most significant step, oxygen atom transfer to the substrate, is the least understood and still quite speculative.

The observation that P-450 with suitable oxygen atom transfer agents will anaerobically oxygenate substrates[3] has spurred much interest in modeling studies using synthetic metalloporphyrins. High-valent metalloporphyrin species can be obtained directly from iron,[4] manganese,[5] and chromium[6] porphyrins with the use of various forms of reduced oxygen. On the basis of these findings, catalytic systems have been devised which oxygenate hydrocarbons in good yields.[7] Shape selective catalysts for both alkane hydroxylation and olefin epoxidation have been discovered[8] by using

(1) (a) Stanford University. (b) CNRS, Toulouse, France.

(2) For a review of the catalytic cycle of cytochrome P-450 see: (a) Coon, M. J.; White, R. E. "Metal Ion Activation of Dioxygen"; Spiro, T. G., Ed.; Wiley: New York, **1980**; pp 73-123. (b) White, R. E.; Coon, M. J. *Annu. Rev. Biochem.* **1980**, *49*, 315-356.

(3) (a) Hrycay, E. G.; O'Brien, P. J. *Arch. Biochem. Biophys.* **1972**, *153*, 480-494. (b) Lichtenberger, F.; Nastainczyk, W.; Ullrich, V. *Biochem. Biophys. Res. Commun.* **1976**, *70*, 939-946.

(4) Groves, J. T.; Haushalter, R. C.; Nakamura, M.; Nemo, T. E.; Evans, B. J. *J. Am. Chem. Soc.* **1981**, *103*, 2884-2886.

(5) (a) Hill, C. L.; Schardt, B. C. *J. Am. Chem. Soc.* **1980**, *102*, 6374-6375. (b) Groves, J. T.; Kruper, W. J., Jr.; Haushalter, R. C. *J. Am. Chem. Soc.* **1980**, *102*, 6375-6377. (c) Schardt, B. C.; Hollander, F. J.; Hill, C. L. *J. Chem. Soc. Chem. Commun.* **1981**, 765-766. (d) Schardt, B. C.; Hollander, F. J.; Hill, C. L. *J. Am. Chem. Soc.* **1982**, *104*, 3964-3972. (e) Smegal, J. A.; Hill, C. L. *J. Am. Chem. Soc.* **1983**, *105*, 2920-2922.

(6) (a) Groves, J. T.; Haushalter, R. C. *J. Chem. Soc., Chem. Commun.* **1981**, 1165-1166. (b) Groves, J. T.; Kruper, W. J., Jr.; Haushalter, R. C.; Butler, W. M. *Inorg. Chem.* **1982**, *21*, 1363-1368.

(7) Examples of iron systems: (a) Groves, J. T.; Nemo, T. E.; Myers, R. S. *J. Am. Chem. Soc.* **1979**, *101*, 1032-1033. (b) Groves, J. T.; Kruper, W. J., Jr.; Nemo, T. E.; Myers, R. S. *J. Mol. Catal.* **1980**, *7*, 169-177. (c) Groves, J. T.; Watanabe, Y.; McMurry, T. J. *J. Am. Chem. Soc.* **1983**, *183*, *105*, 4489-4490. (d) Lindsay-Smith, J. R.; Steath, P. R. *J. Chem. Soc., Perkin Trans. 2* **1982**, 1009-1015. (e) Nee, M. W.; Bruice, T. C. *J. Am. Chem. Soc.* **1982**, *104*, 6123-6125. Manganese systems: (f) Hill, C. L.; Smegal, J. A. *Nouv. J. Chem.* **1982**, *6*, 287-289. (g) Smegal, J. A.; Hill, C. L. *J. Am. Chem. Soc.* **1983**, *105*, 3515-3521. (h) Smegal, J. A.; Schardt, B. C.; Hill, C. L. *J. Am. Chem. Soc.* **1983**, *105*, 3510-3514. (i) Guilmet, E.; Meunier, B. *Tetrahedron Lett.* **1980**, *21*, 4449-4450. (j) Guilmet, E. Meunier, B. *Nouv. J. Chem.* **1982**, *6*, 511-515. (k) Guilmet, E.; Meunier, B. *J. Mol. Catal.* **1984**, *23*, 115-119. Chromium systems: (l) Groves, J. T.; Kruper, W. J., Jr. *J. Am. Chem. Soc.* **1979**, *101*, 7613-7615.

(8) (a) Mansuy, D.; Bartoli, J. F.; Momenteau, M. *Tetrahedron Lett.* **1982**, *23*, 2781-2784. (b) Groves, J. T.; Nemo, T. E. *J. Am. Chem. Soc.* **1983**, *105*, 5786-5791. (c) Groves, J. T.; Myers, R. S. *J. Am. Chem. Soc.* **1983**, *105*, 5791-5796. (d) Groves, J. T.; Nemo, T. E. *J. Am. Chem.Soc.* **1983**, *105*, 6243-6248. (e) Suslick, K. S.; Fox, M. M. *J. Am. Chem. Soc.* **1983**, *105*, 3507-3510. (f) Suslick, K. S.; Cook, B. R.; Fox, M. M. Abstracts of Papers, 187th National Meeting of the American Chemical Society, St. Louis, Missouri, April 8-13, 1984; American Chemical Sciety: Washington, D.C., 1984; INOR 69.

0002-7863/85/1507-2000$01.50/0